Derivation and simulation of the nonlinear dynamics of a flapping wing micro-air vehicle

C. Orlowski*, A. Girard, and W. Shyy
University of Michigan, Department of Aerospace Engineering, 1320 Beal Ave, Ann Arbor, MI USA 48109

ABSTRACT

The paper presents a derivation of the equations of motion for a flapping wing micro-air vehicle. The equations of motion are derived using D'Alembert's Principle extended to rigid bodies. The micro-air vehicle is modeled as a a system of three rigid bodies with rigidly attached wings. Each wing has three separate degrees of freedom: flapping, lagging, and feathering. The MAV is assumed to be operating in an environment with a flat Earth, constant gravity, zero wind, and the MAV has constant mass. The model is simulated using time-averaged aerodynamic force and moment data in a normal hovering mode.

1 NOMENCLATURE

X, Y, Z: components of the position vector of the central body in an inertial frame
ψ, θ, ϕ: 3-2-1 Euler Angles for the orientation of the central body with respect to a inertial frame
α_R, α_L: angle of attack of the right and left wings, respectively (rotation about $\bar{b}_y$ axis)
δ_R, δ_L: flapping angle of the right and left wings, respectively (rotation about $\bar{b}_x$ axis, up and down flapping motion)
ζ_R, ζ_L: lagging angle of the right and left wings respectively (rotation about $\bar{b}_z$ axis, forward and back flapping motion)
u, v, w: components of the translational velocity vector of the central body
p, q, r: components of the angular velocity vector of the central body
$\dot{\alpha_R}$, $\dot{\alpha_L}$: time rate of change of the angle of attack
$\dot{\delta_R}$, $\dot{\delta_L}$: time rate of change of the flapping angle
$\dot{\zeta_R}$, $\dot{\zeta_L}$: time rate of change of the lagging angle
m_1, m_2, m_3: mass of the central body, mass of the right wing and mass of the left wing
$\bar{\rho}_{c2}$, $\bar{\rho}_{c3}$: position vectors from the hinge to the respective wing's center of mass
$\bar{R}$, $\bar{L}$: position vectors of the hinge from the central body center of mass in the B frame
$\bar{b}_x, \bar{b}_y, \bar{b}_z$: unit vectors of the central body-fixed frame, the B frame
Q_j: generalized forces for each generalized coordinate
$\bar{\gamma}_{ij}$: velocity coefficient of the ith body with respect to the jth generalized speed
$\bar{\beta}_{ij}$: angular velocity coefficient of the ith body with respect to the jth generalized speed
$[F_x, F_y, F_z]$: aerodynamics forces in body-fixed coordinates
$[L, M, N]$: aerodynamics moments in body-fixed coordinates
B: body-fixed frame for the central body
H_R: body-fixed frame for the central body, origin at right wing hinge
H_L: body-fixed frame for the central body, origin at left wing hinge
W_R: body-fixed frame for the right wing
W_L: body-fixed frame for the left wing
$\mathbf{I}_1$: inertia tensor for the central body in the B frame
$\mathbf{I}_2$: inertia tensor for the right wing in the W_R frame
$\mathbf{I}_3$: inertia tensor for the left wing in the W_L frame
$\mathbf{I}'_2, \mathbf{I}'_3$: inertia tensors for the right wing and left wing in the H_R and H_L frames
$\mathbf{R}_B$: rotation matrix from inertial frame to B frame using 3-2-1 Euler Angles
$\mathbf{R}_R$: rotation matrix from W_R frame to H_R frame
$\mathbf{R}_L$: rotation matrix from W_L frame to H_L frame
$\mathbf{R}_{\zeta_R}, \mathbf{R}_{\alpha_R}, \mathbf{R}_{\delta_R}$: individual rotation matrices for W_R frame to H_R frame
$\mathbf{R}_{\zeta_L}, \mathbf{R}_{\alpha_L}, \mathbf{R}_{\delta_L}$: individual rotation matrices for W_L frame to H_L frame

2 INTRODUCTION

The goal of the presented research, as well as future work, is to further the knowledge of the dynamic behavior of a flapping wing vehicle and to develop effective control schemes for the operation of a flapping wing vehicle in a relevant environment. The research in the flapping wing field has greatly increased over the past 10 years, especially in aerodynamics [1]. Complex models of flapping wing aerodynamics, to include 3-D effects, have been successfully developed, evaluated and implemented [2, 3]. The next step is to take the knowledge of the complex and unstable aerodynamics and incorporate that knowledge into a successful control scheme, either by nonlinear methods, linear methods, or a combination of both.

In order to successfully implement the control scheme, the development and thorough understanding of the nonlinear dynamics and kinematics is paramount. The paper outlines the development of a dynamic model for a flapping-wing

*Email address(es): contact_cptorlo@umich.edu

MAV. The preliminary goal for vehicle size is a total mass of 30 grams and a total wingspan of approximately 15 centimeters. The method used to derive the equations of motion is D'Alembert's Principle for Multiple Rigid Bodies, which is a hybrid of LaGrangian and Eulerian techniques [4]. The flapping wing MAV is modeled as three rigid bodies (central body, right wing, left wing) with a rigid airframe and rigidly attached wings. The nonlinear dynamics will be incorporated with lift, drag and aerodynamic moment data from models developed in reference [5]. The combination of the nonlinear dynamics and aerodynamics should allow for accurate study of the motion of the vehicle. It will enable the discovery of steady-state flight configurations and the eventual development of effective control schemes.

The paper is organized in the following manner. Section 3 is a brief literature review focusing on the dynamic models and control schemes for a flapping wing micro-air vehicle. Section 4 presents a detailed development of the model with relevant reference frames and the derivation of the nonlinear equations of motion. Section 5 presents the simulation efforts and results, accompanied by the dynamic and aerodynamic models used in the simulation. Section 6 presents Conclusions and Future Work.

3 Literature Review

The majority of the previous work in regards to flapping wing vehicles focuses on the aerodynamics and the interactions of the flapping wings with the fluid flow around the wings. A limited amount of work has been completed in regards to the development of dynamic models and control schemes to successfully operate a flapping wing micro-air vehicle.

Sun and Wang [1] acknowledge that the field of aerodynamics, in regards to insect flight, is highly studied. The main purpose of reference [1] is to produce a quantitative analysis of the stability of hovering flight for a model insect. The authors chose a dynamics model previously given in [6, 7]. The dynamics model chosen is the standard, linearized aircraft dynamics that can be found in [8]. In contrast to the Taylor and Thomas model [7], Sun and Wang use stability and control derivatives calculated by CFD methods. Taylor and Thomas used time average aerodynamics force and moment calculations for a wing beat cycle. The Sun and Wang model limits the model to have six degrees of freedom, but enhances the linearization and simplification of the model with improved accuracy of the aerodynamics, versus the models used by Taylor and Thomas.

The authors choose the equilibrium point for their analysis to be motionless hovering, with no translational or rotational accelerations. The wings need to accelerate to maintain the flight condition. Sun and Wang make further simplifications, given the flight conditions, by only accounting for the x and z translational motion of the model, in addition to the pitching motion and pitch angle, q and θ, respectively. The equilibrium point is determined by balancing the force and moment equations. The stability derivatives are calculated by only taking into account the motion of the wings, for at hovering the aerodynamics of the central body are neglected due to the absence of translational motion. Sun and Wang concluded that the hovering motion can be stabilized using a combination of two of the four available controls ($\delta\Phi$, change in position, $\delta\phi$, change in mean position, α_1, equal change in angle of attack, and α_2, differential change in the angle of attack).

In reference [9], the authors derived the equations of motion for a flapping wing vehicle using Eulerian methods. The central body is modeled as a point mass without mass moments of inertia. The hinge point for both wings is the same and is positioned at the central body. The goal of the paper is to study trajectory guidance, and not exactly implement a control scheme, so the assumptions and model simplifications seem justified. Modeling the central body as a point mass effectively eliminates the rotational considerations of the central body and the coupling effects between the flapping motion of the wings and rotation of the central body. The authors use two body-fixed reference frames, one for each wing. The wings are modeled with three degrees of freedom: plunge (up and down flapping), pitch (angle of attack), and sweep (forward and back flapping). The disadvantage of the two frames, and no central body frame, requires the tracking of the absolute translational and rotational velocity of not only the central body, but both wings as well. Furthermore, velocities calculated in each of the wings' frames will need to be transformed back into the inertial frame, due to the lack of a body-fixed frame at the central body point mass. Additionally, the method chosen requires the calculation of the reaction forces between the wings and the hinges.

The main advantage to the method of deriving the equations of motion chosen in [9] is that it reduces the nonlinearities of the system. There is still rotational motion of the wing, so the nonlinearities associated with Euler's Equations of Motion are still present in the equations of motion. However, the coupling between p, q, and r is non-existent and there is no need to track the Euler Angles of the central body. Furthermore, as undertaken in the paper, the 3-2-1 Euler Angles tracking the orientation of each wing can be directly used as the time rate of change of the pitch, plunge and sweep angles. The dynamics model does not require additional variables to track and transform the motions of the wing into an inertial frame.

In reference [10], Buler, et al., derive the nonlinear equations of motion using the Gibbs-Appel Equations by using ten generalized coordinates, $\mathbf{q}$, and ten quasi-velocities, $\mathbf{w}$, listed below:

$$\mathbf{q} = [x, y, z, \Phi, \Theta, \Psi, \beta_L, \beta_R, \theta_L, \theta_R]$$

$$\mathbf{w} = [U, V, W, P, Q, R, \dot{\beta_L}, \dot{\beta_R}, \dot{\theta_L}, \dot{\theta_R}].$$

The above equations use standard aircraft notation, except in

the case of β (used to denote the flapping angle - motion about the longitudinal axis of the central body) and θ (used to denote the angle of attack of the wings). Buler, et al., limit the flapping kinematics of their model and do not account, or allow for, forward and back (lagging) translation of the wings. Strictly speaking, their model restricts the stroke-plane of the wing beat to a single plane. The model results in a ten degree of freedom, 2nd-order system (or, alternatively, a twenty degree of freedom, 1st-order system). The method of deriving the equations of motion results in the preservation of the numerous, inherent non-linearities present in a flapping wing micro-air vehicle.

The second half of the paper, after outlining the derivation of the equations of model and the aerodynamic model, presents an outline of Linear Control Theory. The authors continue with an analysis of the control of the linearized system previously derived, but do not provide an analytical solution for the linearization. A desired trajectory is assumed and a linearization, and associated Jacobian matrix, is numerically calculated based on the said trajectory. The paper provides coverage of the various control methods at the authors' disposal and their respective shortcomings. The authors use a linear quadratic regulator problem to determine a nominal control input for the flapping wings of the vehicle. In the end, the authors produce simulations of the dynamics of a flapping vehicle/animal, based on the solution of a Newton-Raphson solver to produce the necessary control input vector for the desired output vector.

In reference [11], Bolender derives the nonlinear equations of motion for a flapping wing MAV utilizing Kane's Equations. The main difference from the derivation in reference [11], from other models, is the modeling of the central body as two separate rigid bodies. The central body has a main body, B, and a tail section, T. The tail section is limited to one degree of freedom about the hinge point between body B and body T. The tail section is used for pitch control of the flapping wing MAV. Bolender treats the wings in two separate manners. One treatment ignores the combined mass of the wing. The other treatment accounts for the mass of the wing in the dynamics of the central body. However, in either case, the wings are not treated as having separate degrees of freedom and are considered to be holonomically constrained to the central body. The wings' motion is treated as a prescribed motion. The motion of the wings is a function of time and a control input.

4 Derivation of the Nonlinear Equations of Motion

4.1 D'Alembert's Principle for Multiple Rigid Bodies

The method chosen to derive the equations of motion is D'Alembert's Principle Extended to Multiple Rigid Bodies. A detailed description of the method can be found in [12, 13]. The chosen method is also briefly covered in [4]. The Gibbs-Appell Equations, presented in [10], and Kane's Equations, presented in [11], are both extensions of D'Alembert's Principle [4] and have their own strengths and weaknesses [11]. The statement of D'Alembert's Principle, in [12], is

$$\sum_{i=1}^{n}[m_i(\dot{\bar{\mathbf{v}}}_i+\ddot{\bar{\rho}}_{ci})\cdot\bar{\gamma}_{\mathbf{ij}}+(\mathbf{I_i}\cdot\dot{\bar{\omega}}_{\mathbf{i}}+\bar{\omega}_{\mathbf{i}}\times\mathbf{I_i}\cdot\bar{\omega}_{\mathbf{i}}+m_i\bar{\rho}_{\mathbf{ci}}\times\dot{\bar{\mathbf{v}}}_i)\cdot\bar{\beta}_{\mathbf{ij}}] = Q_j, \tag{1}$$

where i is the number of rigid bodies and j is the number of generalized coordinates. The flapping wing vehicle is modeled as a system of three rigid bodies ($n = 3$): a central fuselage with two rigid wings attached at ideal hinges. The wings and central body are modeled as rigid airframes. A body-fixed frame, frame B, is attached to the central body at its center of mass; the frame is aligned with the $\bar{b}_x$ vector through the nose of the micro-air vehicle, $\bar{b}_y$ is perpendicular to $\bar{b}_x$ and pointed out of the right side of the central body, and $\bar{b}_z$ pointed downward out of of the bottom of the micro-air vehicle. The body-fixed frame is the same as for fixed-wing aircraft and is presented in Figure 1.

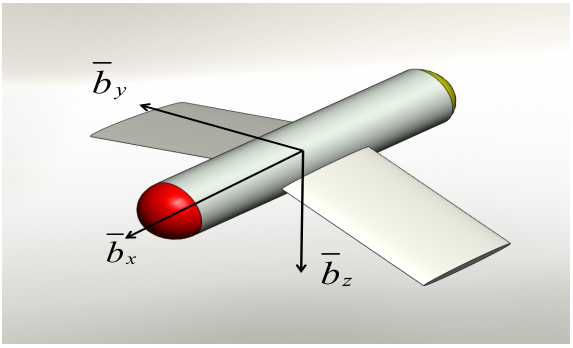

Figure 1: Vehicle Model

The vectors $\bar{\mathbf{R}}$ and $\bar{\mathbf{L}}$ denote position vectors from the central body center of mass to the hinge/attachment points of the wings. At the hinge points, two central body-fixed frames are attached, with directions parallel to the central body B frame. The H_R frame is fixed with origin at the right wing hinge point. The H_L frame is fixed with origin at the left wing hinge point. Since the central body is modeled as a rigid body, the magnitude and components of $\bar{\mathbf{R}}$ and $\bar{\mathbf{L}}$ are constant. We define the individual components of $\bar{\mathbf{R}}$ and $\bar{\mathbf{L}}$ as

$$\bar{\mathbf{R}} = \begin{bmatrix} R_x & R_y & R_z \end{bmatrix} \tag{2}$$

and

$$\bar{\mathbf{L}} = \begin{bmatrix} L_x & L_y & L_z \end{bmatrix}. \tag{3}$$

The vectors $\bar{\rho}_{c2}$ and $\bar{\rho}_{c3}$ denote the vectors from the hinge points on the central body to the respective centers of mass for each wing ($\bar{\rho}_{c2}$ for the right wing and $\bar{\rho}_{c3}$ for the left wing). The magnitude of the $\bar{\rho}_{ci}$ vectors is constant, based on the assumption of rigid bodies and rigidly attached wings. A wing-fixed frame is attached to each wing at the hinge point. The

origin of the winged fixed frames is the hinge point and when the wings at are their respective initial positions, the axes of the wing-fixed frames, W_R and W_L, are parallel with the central body-fixed frame B, and are identical to the hinge frames, H_R and H_L. The frames W_R and W_L and the vectors $\bar{R}$, $\bar{L}$, $\bar{\rho}_{c2}$, and $\bar{\rho}_{c3}$ are presented in Figure 2.

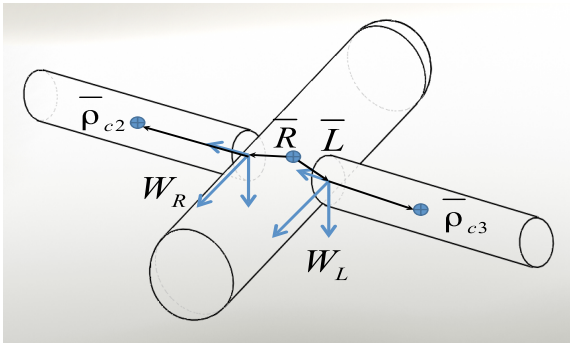

Figure 2: Wing Frames

The motion of the center of mass of the wings is tracked similar to a mass moving in spherical coordinates, with a constant radius, fixed at the origin of the system. In this case, the origin of the respective motion is the hinge point, which is coincident with the origin of the W_R, H_R, H_L and W_L frames. The constant radius is the magnitude of the vectors, $\bar{\rho}_{c2}$ and $\bar{\rho}_{c3}$. The center of mass of the wing is assumed to be along the y-axis of the hinge frames when the wing angles are identically zero. The position of the centers of mass of each wing are expressed by the following vectors:

$$\bar{\rho}_{c2} = \rho_{c2}[\cos\delta_R \sin\zeta_R \bar{b}_x + \cos\delta_R \cos\zeta_R \bar{b}_y + \sin\delta_R \bar{b}_z] \quad (4)$$

$$\bar{\rho}_{c3} = \rho_{c3}[\cos\delta_L \sin\zeta_L \bar{b}_x - \cos\delta_L \cos\zeta_L \bar{b}_y + \sin\delta_L \bar{b}_z]. \quad (5)$$

Developing equations of motion using D'Alembert's Principle for Rigid Bodies requires the selection of reference points for each rigid body. The reference point for the central body, rigid body 1, is it's respective center of mass. The reference points for the right and left wing are chosen to be the hinge attachment points, located on the central body. The vectors tracking the center of mass of the wings in the hinged-fixed frames are the vectors $\bar{\rho}_{c2}$ and $\bar{\rho}_{c3}$. The required acceleration vectors of $\ddot{\bar{\rho}}_{c2}$ and $\ddot{\bar{\rho}}_{c3}$ are derived using diligent application of the chain rule.

There are three main advantages to selecting D'Alembert's Principle. First, by taking the hinge points as reference points, the requirement to calculate the reaction forces between the wings and the central body is eliminated. Second, the mass moments of inertia of the wings need to be initially calculated about the reference points. The mass moments of inertia will remain constant in the wing-fixed frames and do not need to be translated into the B frame [12]. Third, by choosing reference points on the central body, the absolute velocity of the wings does not need to be tracked.

In order to successfully develop the equations of motion, the generalized coordinates and quasi-velocities need to be specified. In this formulation, the twelve generalized coordinates are chosen to be the following: X, Y, Z (inertial position of central body), ψ, θ, ϕ (3-2-1 Euler Angles of central body), δ_R, α_R, ζ_R, δ_L, α_L, ζ_L. The twelve quasi-velocities are the following: u, v, w, p, q, r, $\dot{\delta}_R$, $\dot{\alpha}_R$, $\dot{\zeta}_R$, $\dot{\delta}_L$, $\dot{\alpha}_L$, and $\dot{\zeta}_L$. To summarize, the generalized coordinates, q, are

$$\mathbf{q}_j = [X, Y, Z, \psi, \theta, \phi, \delta_R, \alpha_R, \zeta_R, \delta_L, \alpha_L, \zeta_L] \quad (6)$$

and the quasi-velocites, $\mathbf{u}_j$, are

$$\mathbf{u}_j = [u, v, w, p, q, r, \dot{\delta}_R, \dot{\alpha}_R, \dot{\zeta}_R, \dot{\delta}_L, \dot{\alpha}_L, \dot{\zeta}_L]. \quad (7)$$

The importance of flapping and lagging angles, and the associated degrees of freedom, is important when biological flyers transition from hovering to forward flight [2]. Figures 3, 4, and 5 show the vehicle model from different view points and the relationship of the wing frames, W_R and W_L, and the central body frame B. The left side of the vehicle, and α_L, is not depicted, but is simply the mirror image of Figure 4. Dashed lines represent a negative direction in the respective reference frame. The flapping angles, δ_R and δ_L, are positive in a downward motion (positive $\bar{b}_z$). The lagging angles, ζ_R and ζ_L are positive in a forward flapping motion (positive $\bar{b}_x$). The hinge frames, H_R and H_L, are not depicted, but are parallel to the B frame.

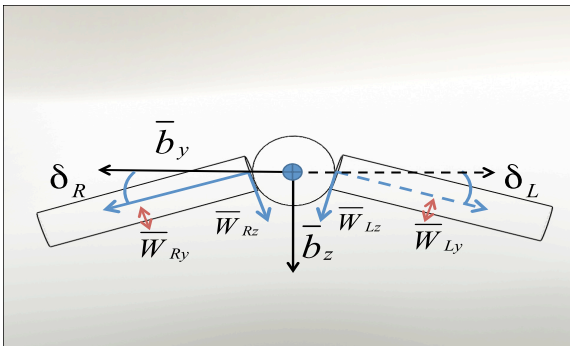

Figure 3: Front View - δ_R and δ_L

4.2 *Velocity and Angular Velocity Coefficients*

The first step in the derivation is to determine the velocity coefficients, $\bar{\gamma}_{ij} = \frac{\partial \bar{v}_i}{\partial u_j}$, and the angular velocity coefficients, $\bar{\beta}_{ij} = \frac{\partial \bar{\omega}_i}{\partial u_j}$, where i denotes the rigid body and j denotes the generalized speeds. The translational and rotational velocities of each of the rigid bodies are

$$\begin{aligned} \bar{\mathbf{v}}_1 &= u\bar{b}_x + v\bar{b}_y + w\bar{b}_z \\ \bar{\mathbf{v}}_2 &= \bar{\mathbf{v}}_1 + \bar{\omega}_1 \times \bar{\mathbf{R}} \\ \bar{\mathbf{v}}_3 &= \bar{\mathbf{v}}_1 + \bar{\omega}_1 \times \bar{\mathbf{L}} \end{aligned} \quad (8)$$

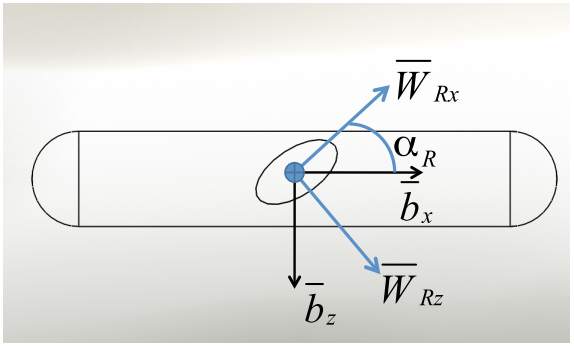

Figure 4: Right Side View - α_R

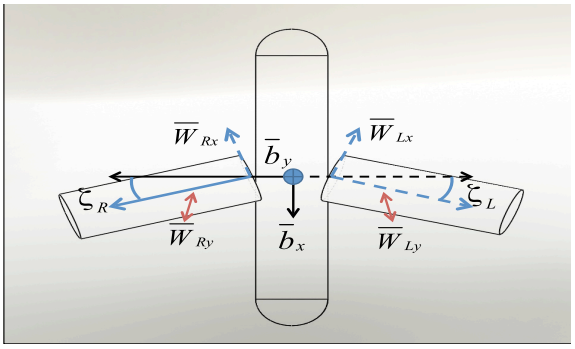

Figure 5: Top View - ζ_R and ζ_L

and

$$\begin{aligned}\bar{\omega}_{\mathbf{1}} &= p\bar{b}_x + q\bar{b}_y + r\bar{b}_z \\ \bar{\omega}_{\mathbf{2}} &= (p+\dot{\delta}_R)\bar{b}_x + (q+\dot{\alpha}_R)\bar{b}_y + (r-\dot{\zeta}_R)\bar{b}_z \\ \bar{\omega}_{\mathbf{3}} &= (p-\dot{\delta}_L)\bar{b}_x + (q+\dot{\alpha}_L)\bar{b}_y + (r+\dot{\zeta}_L)\bar{b}_z\end{aligned} \quad . \tag{9}$$

The velocity and angular velocity coefficients are obtained by taking the partial derivatives of $\bar{\mathbf{v}}_i$ and $\bar{\omega}_i$ with respect to the generalized speeds. The velocity coefficients, $\bar{\gamma}_{1j}$, and the angular velocity coefficients, $\bar{\beta}_{1j}$ for generalized speeds $j = 1 \ldots 6$ of the central body are

$$\bar{\gamma}_{1j} = \begin{bmatrix} \bar{b}_x & \bar{b}_y & \bar{b}_z & 0 & 0 & 0 \end{bmatrix} \tag{10}$$

and

$$\bar{\beta}_{1j} = \begin{bmatrix} 0 & 0 & 0 & \bar{b}_x & \bar{b}_y & \bar{b}_z \end{bmatrix}. \tag{11}$$

The velocity and angular velocity coefficients of the central body for coordinates $j = 7 \ldots 12$ are identically zero. The velocity coefficients for the right wing, $\bar{\gamma}_{2j}$, and the left wing, $\bar{\gamma}_{3j}$, for $j = 1 \ldots 6$ are

$$\begin{aligned}\bar{\gamma}_{2j} = [&\bar{b}_x \quad \bar{b}_y \quad \bar{b}_z \ldots \\ &-R_z\bar{b}_y + R_y\bar{b}_z \quad R_z\bar{b}_x - R_x\bar{b}_z \quad -R_y\bar{b}_x + R_x\bar{b}_y]\end{aligned} \tag{12}$$

$$\begin{aligned}\gamma_{3j} = [&\bar{b}_x \quad \bar{b}_y \quad \bar{b}_z \ldots \\ &-L_z\bar{b}_y + L_y\bar{b}_z \quad L_z\bar{b}_x - L_x\bar{b}_z \quad -L_y\bar{b}_x + L_x\bar{b}_y].\end{aligned} \tag{13}$$

The velocity coefficients for the left and right wing, for $j = 7 \ldots 12$ are identically zero. The angular velocity coefficients of the right and left wings, $\bar{\beta}_{2j}$ and $\bar{\beta}_{3j}$, respectively, are identically zero for $j = 1 \ldots 3$. For the right wing, $\bar{\beta}_{2j}$ is identically zero for $j = 10 \ldots 12$. For the left wing, $\bar{\beta}_{3j}$ is identically zero for $j = 7 \ldots 9$. For quasi-velocities $j = 4 \ldots 6$, the angular velocity coefficients are

$$\bar{\beta}_{2j} = \begin{bmatrix} \bar{b}_x & \bar{b}_y & \bar{b}_z \end{bmatrix} \tag{14}$$

$$\bar{\beta}_{3j} = \begin{bmatrix} \bar{b}_x & \bar{b}_y & \bar{b}_z \end{bmatrix}. \tag{15}$$

For the right wing, with respect to coordinates $j = 7 \ldots 9$, the angular velocity coefficients are

$$\bar{\beta}_{2j} = \begin{bmatrix} \bar{b}_x & \bar{b}_y & -\bar{b}_z \end{bmatrix}. \tag{16}$$

In regards to the left wing, the angular velocity coefficients for $j = 10 \ldots 12$ are

$$\bar{\beta}_{3j} = \begin{bmatrix} -\bar{b}_x & \bar{b}_y & \bar{b}_z \end{bmatrix}. \tag{17}$$

The accelerations of the three rigid bodies are obtained by differentiating the translational and rotational velocities and making proper use of the transport theorem [4]. For example, the acceleration of the right wing, $\dot{\bar{\mathbf{v}}}_2$ in the central body frame, is

$$\dot{\bar{\mathbf{v}}}_2 = \dot{\bar{\mathbf{v}}}_1 + \dot{\bar{\omega}}_1 \times \bar{\mathbf{R}} + \bar{\omega}_1 \times \bar{\mathbf{v}}_1 + \bar{\omega}_1 \times (\bar{\omega}_1 \times \bar{\mathbf{R}}). \tag{18}$$

4.3 Inertia Tensors

For the central body, an $x - z$ plane of mass symmetry is assumed. No planes of mass symmetry are assumed for either wing during the model development. As a result, the resulting mass moments of inertia matrices for each rigid body are the following:

$$\mathbf{I_1} = \begin{bmatrix} I_{xx,1} & 0 & -I_{xz,1} \\ 0 & I_{yy,1} & 0 \\ -I_{xz,1} & 0 & I_{zz,1} \end{bmatrix} \tag{19}$$

$$\mathbf{I_2} = \begin{bmatrix} I_{xx,2} & -I_{xy,2} & -I_{xz,2} \\ -I_{xy,2} & I_{yy,2} & -I_{yz,2} \\ -I_{xz,2} & -I_{yz,2} & I_{zz,2} \end{bmatrix} \tag{20}$$

$$\mathbf{I_3} = \begin{bmatrix} I_{xx,3} & -I_{xy,3} & -I_{xz,3} \\ -I_{xy,3} & I_{yy,3} & -I_{yz,3} \\ -I_{xz,3} & -I_{yz,3} & I_{zz,3} \end{bmatrix}. \tag{21}$$

4.4 Rotation Matrices

Although it is not necessary to continuously calculate the mass moments of inertia for the wings in the B frame, it may be necessary in the use of the model to rotate aerodynamic forces generated by the flapping of the wings from the W_R and W_L frames into the B frame. $\mathbf{R}_R$ is the rotation matrix

of the W_R frame into the H_R frame. Treating the angles describing the orientation of the right wing, ζ_R, α_R, and δ_R, as 3-2-1 Euler Angles results in the calculation of $\mathbf{R}_R$.

$$\mathbf{R}_{\zeta_R} = \begin{bmatrix} \cos\zeta_R & \sin\zeta_R & 0 \\ -\sin\zeta_R & \cos\zeta_R & 0 \\ 0 & 0 & 1 \end{bmatrix}$$

$$\mathbf{R}_{\alpha_R} = \begin{bmatrix} \cos\alpha_R & 0 & -\sin\alpha_R \\ 0 & 1 & 0 \\ \sin\alpha_R & 0 & \cos\alpha_R \end{bmatrix}$$

$$\mathbf{R}_{\delta_R} = \begin{bmatrix} 1 & 0 & 0 \\ 0 & \cos\delta_R & \sin\delta_R \\ 0 & -\sin\delta_R & \cos\delta_R \end{bmatrix}$$

$$\mathbf{R}_R = \mathbf{R}_{\delta_R}\mathbf{R}_{\alpha_R}\mathbf{R}_{\zeta_R}. \tag{22}$$

A similar procedure can be utilized to obtain the rotation of aerodynamic forces and moments generated by the left wing into the B frame. The rotation matrix for the left wing is

$$\mathbf{R}_L = \mathbf{R}_{\delta_L}\mathbf{R}_{\alpha_L}\mathbf{R}_{\zeta_L}. \tag{23}$$

The rotation matrix R_{α_L} has the same structure as it's counterpart on the right wing, R_{α_R}. The rotation matrices R_{ζ_L} and R_{δ_L} are different and are defined as

$$\mathbf{R}_{\zeta_L} = \begin{bmatrix} \cos(\pi-\zeta_L) & \sin(\pi-\zeta_L) & 0 \\ -\sin(\pi-\zeta_L) & \cos(\pi-\zeta_L) & 0 \\ 0 & 0 & 1 \end{bmatrix} \tag{24}$$

$$\mathbf{R}_{\delta_L} = \begin{bmatrix} 1 & 0 & 0 \\ 0 & \cos(\pi+\delta_L) & \sin(\pi+\delta_L) \\ 0 & -\sin(\pi+\delta_L) & \cos(\pi+\delta_L) \end{bmatrix}. \tag{25}$$

By using the trigonometric rules for sine and cosine, the rotation matrices R_{ζ_L} and R_{δ_L} simplify to

$$\mathbf{R}_{\zeta_L} = \begin{bmatrix} -\cos\zeta_L & -\sin\zeta_L & 0 \\ \sin\zeta_L & -\cos\zeta_L & 0 \\ 0 & 0 & 1 \end{bmatrix} \tag{26}$$

and

$$\mathbf{R}_{\delta_L} = \begin{bmatrix} 1 & 0 & 0 \\ 0 & -\cos\delta_L & -\sin\delta_L \\ 0 & \sin\delta_L & -\cos\delta_L \end{bmatrix}. \tag{27}$$

4.5 Force Description

The aerodynamics forces and moments produced by the wings are assumed to act over the three bodies as a whole. The aerodynamic forces,F_{aero}, are defined as

$$F_{aero} = F_x\bar{b}_x + F_y\bar{b}_y + F_z\bar{b}_z. \tag{28}$$

The aerodynamic moments, M_{aero}, are defined as

$$M_{aero} = L\bar{b}_x + M\bar{b}_y + N\bar{b}_z. \tag{29}$$

The generalized forces, Q_i, are determined using the principle of virtual work. Constraint forces do not perform virtual work, therefore they are not considered in the formulations. The generalized forces affecting the translation of the central body are

$$\begin{bmatrix} Q_1 \\ Q_2 \\ Q_3 \end{bmatrix} = \begin{bmatrix} F_x \\ F_y \\ F_z \end{bmatrix} + (m_1+m_2+m_3)\mathbf{R}_B \begin{bmatrix} 0 \\ 0 \\ g \end{bmatrix}. \tag{30}$$

The generalized forces/moments affecting the rotation of the central body are

$$\begin{bmatrix} Q_4 \\ Q_5 \\ Q_6 \end{bmatrix} = \begin{bmatrix} L \\ M \\ N \end{bmatrix} + (\bar{\mathbf{R}} + \bar{\rho}_{c2}) \times (m_2)\mathbf{R}_B \begin{bmatrix} 0 \\ 0 \\ g \end{bmatrix} + \ldots + (\bar{\mathbf{L}} + \bar{\rho}_{c3}) \times (m_3)\mathbf{R}_B \begin{bmatrix} 0 \\ 0 \\ g \end{bmatrix}. \tag{31}$$

The generalized forces Q_7, Q_8, and Q_9 are the control moments for the right wing, Q_{10}, Q_{11}, Q_{12} are the control moments for the left wing. Q_8 and Q_{11} control the angle of attack of the wings, right and left wing respectively. Q_7 and Q_{10} control the flapping motion of the wings, while Q_9 and Q_{12} control the lagging angle of the wings.

4.6 Final Equations of Motion

The derived equations of motion, with all of the individual pieces put together, are presented in vector/matrix notation. The first three equations describe the translational velocity of the central body.

$$m_1\dot{\bar{\mathbf{v}}}_{\mathbf{1}} + m_2(\dot{\bar{\mathbf{v}}}_{\mathbf{2}} + \ddot{\bar{\rho}}_{\mathbf{c2}}) + m_3(\dot{\bar{\mathbf{v}}}_{\mathbf{3}} + \ddot{\bar{\rho}}_{\mathbf{c3}}) = \begin{bmatrix} Q_1 \\ Q_2 \\ Q_3 \end{bmatrix}. \tag{32}$$

Due to the continuous flapping of the wings, the rotational dynamics of the central body are the most complex.

$$\mathbf{I_1}\dot{\bar{\omega}}_{\mathbf{1}} + \bar{\omega}_{\mathbf{1}} \times \mathbf{I_1}\bar{\omega}_{\mathbf{1}} + m_2\bar{\mathbf{R}} \times (\dot{\bar{\mathbf{v}}}_{\mathbf{2}} + \ddot{\bar{\rho}}_{\mathbf{c2}}) + m_3\bar{\mathbf{L}} \times (\dot{\bar{\mathbf{v}}}_{\mathbf{3}} + \ddot{\bar{\rho}}_{\mathbf{c3}}) + \ldots$$

$$\mathbf{I_2}\dot{\bar{\omega}}_{\mathbf{2}} + \bar{\omega}_{\mathbf{2}} \times \mathbf{I_2}'\bar{\omega}_{\mathbf{2}} + m_2\bar{\rho}_{\mathbf{c2}} \times \dot{\bar{\mathbf{v}}}_{\mathbf{2}} + \ldots$$

$$\mathbf{I_3}\dot{\bar{\omega}}_{\mathbf{3}} + \bar{\omega}_{\mathbf{3}} \times \mathbf{I_3}\bar{\omega}_{\mathbf{3}} + m_3\bar{\rho}_{\mathbf{c3}} \times \dot{\bar{\mathbf{v}}}_{\mathbf{3}} = \begin{bmatrix} Q_4 \\ Q_5 \\ Q_6 \end{bmatrix}. \tag{33}$$

The rotations of the right wing and and the left wing are described by Equation 34 and Equation 35, respectively.

$$\mathbf{I_2}\dot{\bar{\omega}}_{\mathbf{2}} + \bar{\omega}_{\mathbf{2}} \times \mathbf{I_2}\bar{\omega}_{\mathbf{2}} + m_2\bar{\rho}_{\mathbf{c2}} \times \dot{\bar{\mathbf{v}}}_{\mathbf{2}} = \begin{bmatrix} Q_7 \\ Q_8 \\ Q_9 \end{bmatrix} \tag{34}$$

$$\mathbf{I_3}\dot{\bar{\omega}}_3 + \bar{\omega}_{\mathbf{3}} \times \mathbf{I_3}\bar{\omega}_{\mathbf{3}} + m_3\bar{\rho}_{\mathbf{c3}} \times \dot{\bar{\mathbf{v}}}_{\mathbf{3}} = \begin{bmatrix} Q_{10} \\ Q_{11} \\ Q_{12} \end{bmatrix}. \tag{35}$$

5 SIMULATIONS AND RESULTS

5.1 Model

Through the derivations of the equations of motion, we determined simplications could be made to the model in order to reduce the coupling of the rotations of the wings with the translational and rotational motion of the central body . One of the simplications is to place the hinge points co-linear with the y-axis of the central body. With the hinge points along the y-axis, the x and z components of the $\bar{\mathbf{R}}$ and $\bar{\mathbf{L}}$ vectors are identically zero.

5.2 Aerodynamic Data

The aerodynamic data is obtained by surrogate modeling of two dimensional flow [5]. The model of the wings used to obtained the time-averaged aerodynamics data is a flat plate, with a prescribed chord length, c, and a span of $2c$(for each wing). The plate has a thickness of 2%. To model the mass moments of inertia of the wings, all cross products of inertia are assumed to be zero in the wing frame (when the δ and ζ angles are identically zero). The resulting inertia tensor for the right wing, with zero flapping motion, at the center of mass of the wing in the wing-fixed frame, is

$$\mathbf{I}_2 = \begin{bmatrix} \frac{1}{12}m_2b^2 & 0 & 0 \\ 0 & \frac{1}{12}m_2c^2 & 0 \\ 0 & 0 & \frac{1}{12}m_2(b^2+c^2) \end{bmatrix}, \quad (36)$$

where b is the span of the wing and c is the chord length.

The aerodynamic data [2, 5] prescribes the plunging amplitude as

$$\begin{matrix} \zeta_R(t) = h_a \sin(2\pi f t) \\ \zeta_L(t) = h_a \sin(2\pi f t) \end{matrix} . \quad (37)$$

As previously stated, the wings motion is defined as positive when the lagging motion is in the positive x direction in the body frame. The angle of attack (or rotation of the wing) is described as

$$\alpha(t) = \alpha_o - \alpha_a \sin(2\pi f t + \phi_\alpha). \quad (38)$$

The phase lag between the translation and rotation of the wing is denoted by ϕ_α. In Equation 38, α_o is the initial angle of attack at the start of the flapping motion and α_a is the time-average angle of attack. For the aerodynamic model, the parameters h_a, α_a, and ϕ_α are variable. For a given Reynolds number, the frequency of the flapping can be calculated based on the relationship, from reference [5, 2]

$$Re_{hovering} = \frac{(2\pi f h_a)c}{\nu}. \quad (39)$$

The current aerodynamic data is only for a normal hovering mode, the wing translation is purely horizontal with the respect to the B frame [2]. In the normal hovering mode, the flapping angle (δ_R, δ_L) is identically zero for all time, t.

The control moments for each wing are calculated based on the required accelerations, based on the flapping kinematics, and the inertia tensor in the B frame. They are related by the relationship

$$\begin{bmatrix} Q_7 \\ Q_8 \\ Q_9 \end{bmatrix} = \mathbf{I_2}'\bar{\alpha}_{wing} + \bar{\omega}_2 \times \mathbf{I}_2{}'\bar{\omega}_2 \quad (40)$$

where

$$\bar{\alpha}_{wing} = \begin{bmatrix} 0 \\ \alpha_a(2\pi f)^2 \sin(2\pi f t + \phi_\alpha) \\ -h_a(2\pi f)^2 \sin(2\pi f t) \end{bmatrix}. \quad (41)$$

SImilarly, the control moments for the left wing are

$$\begin{bmatrix} Q_{10} \\ Q_{11} \\ Q_{12} \end{bmatrix} = \mathbf{I_3}'\bar{\alpha}_{wing} + \bar{\omega}_3 \times \mathbf{I}_3{}'\bar{\omega}_3. \quad (42)$$

5.3 Model Parameters

The initial simulations are conducted based off of the current aerodynamic data and do not specifically replicate, or model, any living organism. Based on the aerodynamic data available in [5], a given set of wing kinematics is chosen. For the purpose of the simulations, Case 11 from [5] is used. The C_L is 0.46 from Case 11 and the plunging amplitude is related to the chord length by the ratio [5]

$$\frac{2h_a}{c} = 4.0. \quad (43)$$

The chosen phase angle,ϕ_α, is 90 degrees and the average angle of attack, α_a, is 62.5 degrees ϕ_α and α_a. The Reynolds number for Case 11 is 100. The chord length is calculated by choosing a frequency and utilizing Equation 39. Choosing a frequency of 30 Hz, with a Reynolds number of 100, results in a chord length, c, of 2 mm. The simulations are intended to model a normal hovering mode. Based on the this assumption, the time-averaged aerodynamic moments are assumed to be identically zero. Additionally, the time-averaged coefficient of drag, C_D, is also zero, based on [5]. The lift forces are assumed to counteract the gravity forces acting on the central body.

5.4 Results

Figures 6 and 7 shows the position of the center of mass of the MAV in the B frame. The simulations of the model produce symmetrical flapping. With flapping motion that consists only of lagging and pitching motions, the center of mass of the system symmetrically fore and aft in the B frame. The shift of the center of mass is small. It is on the order of 10^{-7}, which is approximately four orders of magnitude smaller than the vehicle scale.

The Euler angles of the central body are presented in Figures 8, 9 and 10. The results show that the central body

pitches up and down about the $\bar{b}_y$ axis with each wing beat. As the wings go forward, the nose pitches down. The hover is unstable, as the angular velocity of the MAV continues to increase. The bank angle, ϕ, and yaw angle, ψ, are effectively zero. The values produced by the simulation are on the order of 10^{-17} and the error from zero is attributed to simulation error. The pitch angle change is approximately 0.01 radians per flapping cycle. The small effects on the body of each wingbeat, coupled with unstable hover, are consistent with the results in Reference [14].

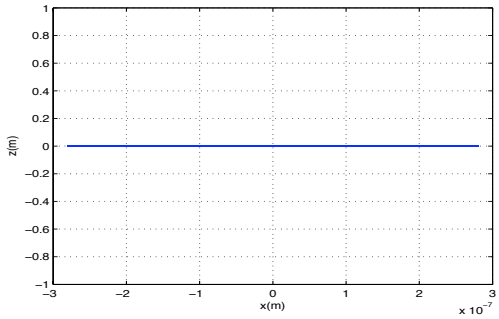

Figure 6: MAV Center of Mass in B Frame - x v. z

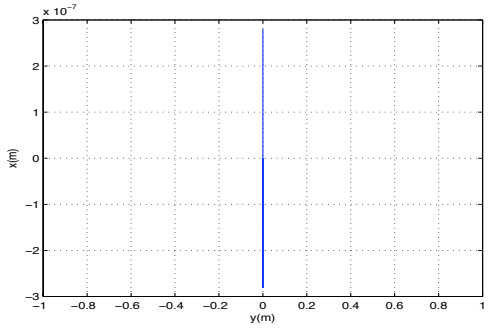

Figure 7: MAV Center of Mass in B Frame - y v. x

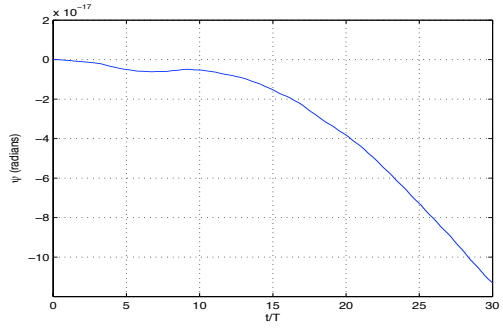

Figure 8: Yaw angle, ψ, of central body

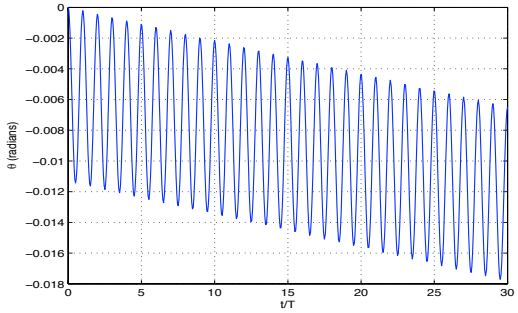

Figure 9: Pitch angle, θ, of central body

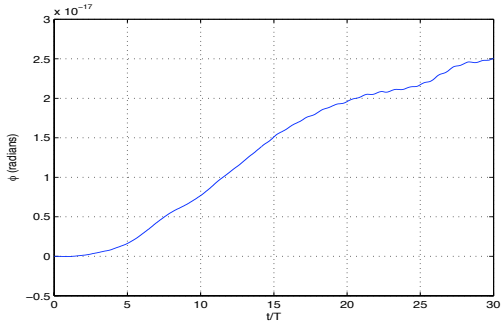

Figure 10: Roll angle, ϕ, of central body

6 Conclusion and Future Work

The paper presented the derivation of the nonlinear, multiple body equations of motion for a flapping wing micro air vehicle using D'Alembert's Principle for Multiple Rigid Bodies. The equations were derived using 12 generalized coordinates and 12 quasi-velocities. Simulations were conducted using time-averaged data for the aerodynamic forces and moments. Future Work will investigate the difference in performance and simulation results between time-averaged data and instantaneous lift and drag data. Previous work has shown in [3, 15] that flexible wings produce more thrust. Hummingbirds control part of their flapping motion [16] by changing the chord length, along the span of the wing, during flapping. Simulations will be conducted with varying positions of the hinge points, the conjecture is that stability may be improved by ensuring that the time-variant system center of mass is forward of the time-variant aerodynamic center. Investigation of nonlinear and linear control schemes will be conducted. Based on the work presented in [10], analytical equilibrium solutions may not exist. Numerical solvers may be required to obtain equilibrium solutions for desired maneuvers and trajectories and to develop control schemes based on the numerical solutions.

ACKNOWLEDGEMENTS

Thanks to Professor Donald T. Greenwood for assistance with the development of the dynamical model. Thanks go to Pat Trizila for assistance with the aerodynamic modeling and integration of the data into the dynamic and kinematic model.

REFERENCES

[1] M. Sun and J.K. Wang. Flight stabilization control of a hovering model insect. *The Journal of Experimental Biology*, 210:2714–2722, 2007.

[2] W. Shyy, Y. Lian, J. Tang, D. Viieru, and H. Liu. *Aerodynamics of low Reynolds number flyers*. Cambridge University Press, New York, NY, 2008.

[3] W. Shyy, Y. Lian, J. Tang, H. Liu, P. Trizilia, B. Stanford, L. Bernal, C. Cesnik, P. Friedmann, and P. Ifju. Computational aerodynamics of low reynolds number, plunging, pitching and flexible wings for mav applications. *Acta Mechanica Sin*, 24:351–373, 2008.

[4] H. Baruh. *Analytical Dynamics*. WCB McGraw-Hill, Boston, MA, 2006.

[5] P. Trizilia, C. Kang, M. Visbal, and W. Shyy. Low reynolds number hovering wing aeroydynamics: performance, tip vortices, and induced jet. *Submitted to Journal of Fluid Mechanics*, 2009.

[6] M. Sun and Y. Xiong. Dynamic flight stability of a hovering bumblebee. *The Journal of Experimental Biology*, 208:447–459, 2005.

[7] G. Taylor and A. Thomas. Dynamic flight stability in the desert locus *Schistocerca gregaria*. *The Journal of Experimental Biology*, 206:2803–2829, 2003.

[8] B. Etkin and L.D. Reid. *Dynamics of flight*. John Wiley and Sons, New York, NY, 1996.

[9] J. Jackson, R. Bhattacharya, and T. Strganac. Modelling and suboptimal trajectory generation for a symmetric flapping wing vehicle. In *Proceedings of the AIAA Guidance, Navigation, and Control Conference and Exhibit, Honolulu, Hawaii, USA, 18-21 August 2008*. American Institute of Aeronautics and Astronautics, 2008.

[10] W. Buler, L. Loroch, K. Sibilski, and A. Zyluk. Modeling and simulation of the nonlinear dynamic behavior of a flapping wings micro-aerial-vehicle. In *Proceedings of the 42nd AIAA Aerospace Sciences Meeting and Exhibit, Reno, Nevada, USA, 5-8 November 2004*. American Institute of Aeronautics and Astronautics, 2004.

[11] M. A. Bolender. Rigid multi-body equations-of-motion for flapping wing mavs using kane's equations. In *Accepted for AIAA Guidance, Navigation and Control Conference, 10-13 August 2009, Chicago, IL*. American Institute of Aeronautics and Astronautics, 2009.

[12] D. T. Greenwood. *Principles of dynamics*. Prentice Hall, Upper Saddle River, NJ, 1988.

[13] D. T. Greenwood. *Advanced dynamics*. Cambridge University Press, 2006.

[14] M. Sun, P. Liu, and K.Wang. Dynamic flight stability of a hovering hoverfly. In *Proceedings of the Fifth International Conference on Fluid Mechanics, Aug. 15-19, 2007, Shanghai, China*. Tsinghua University Press and Springer, 2007.

[15] H. Aono, S. Chimakurthi, C. Cesnik, H. Liu, and W. Shyy. Computational modeling of spanwise flexibility effects on flapping wing aerodynamics. In *Proceedings of the 47th AIAA Aerospace Sciences Meeting including the The New Horizons Forum and Aerospace Exposition, Orlando, Florida, Jan 5-8, 2009*, volume 2009-1270. American Institute of Aeronautics and Astronautics, 2009.

[16] B. Tobalske, D. Warrick, C. Clark, D. Powers, T. Hedrick, G. Hyder, and A. Biewener. Three-dimensional kinematics of hummingbird flight. *The Journal of Experimental Biology*, 210:2368–2382, 2007.